J. Mater. Shaping Technol. (1991) 9:103–115

Plasticity Theory for Working of Porous Metals

J. Duszczyk

Abstract. The consideration of different shapes of the yield surface during the compaction of porous materials indicates that an ellipsoid should be recommended due to its simple mathematical form and close description of the actual behaviour of powdered metal (PM) materials during forming processes. Such a yield surface described by a new yield function is discussed for the 7XXX series PM rapidly solidified aluminum alloy. The function is applied to derivation of upper bound theory for porous metals. This paper emphasizes the experimental approach to the determination of the coefficients for this function, relating them to the properties of porous materials (density) and forming conditions (pressure, temperature, strain rate). The yield function and flow rules are verified by cold isostatic pressing and simple hot uniaxial compaction with a satisfactory level of correlation between the experimental and estimated results. The assumption in the upper bound approach that the porous body may be characterized by the existence of displacement rate discontinuities is judged by microstructures, hardness, and density throughout the deformation zone during extrusion.

Introduction

It is important for the optimization of consolidation processes of components produced by the powder technology route to consider a wider application of computer modelling techniques. This goal can be achieved if the reasonably general plasticity theory for porous materials will be developed. Unfortunately this goal has not been reached so far due to very complicated mechanical, rheological and metallurgical aspects involved in the description of the behaviour of powders during cold or hot forming processes. The modelling of the consolidation of porous billets requires a new yield function, which differs from the Huber-Mises function due to a change in volume of the porous body during compaction.

Therefore the flow of porous material depends on the hydrostatic stress σ_m (or the first invariant of the stress tensor J_1: $J_1 = 3\sigma_m = \sigma_1 + \sigma_2 + \sigma_3$). In general the yield function for porous materials should include J_1 and the second invariant of the deviatoric stress tensor $J_2' = (1/6)[(\sigma_1 - \sigma_2)^2 + (\sigma_2 - \sigma_3)^2 + (\sigma_3 - \sigma_1)^2]$.

Therefore:

$$F = f(J_2', J_1) \tag{1}$$

The assumption of a shape of the yield surface is very important because it influences the description of a plastic potential g and flow rules. The yield surface for porous materials must be smooth, convex, and close. Moreover it has to fulfil the following condition: as a relative density of porous body ρ (the ratio between density of the porous body and theoretical density of a solid nonporous material) increases, the yield surface of PM material must approach the Huber-Mises cylinder, taking this shape at $\rho = 1$.

Considering geometrical representation of the yield function in $(3J_2')^{1/2}/\sigma_f - J_1/\sigma_f$ coordinates (σ_f = the yield stress of any material) (Fig. 1), one has to recognize that the yield locus determines not only the

The author is with Laboratory of Materials Science, Delft University of Technology, Rotterdamseweg 137, 2628 AL Delft, The Netherlands.

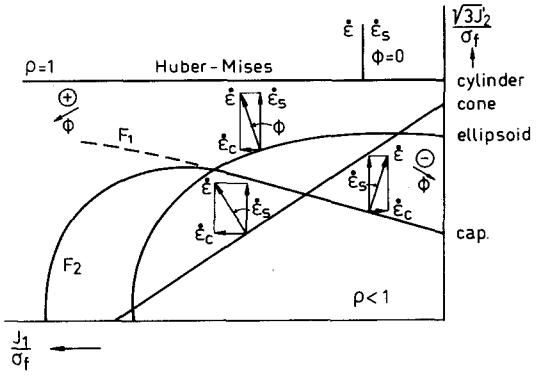

Fig. 1. Geometrical representation of different forms of yield function during compaction.

stress conditions for which a flow occurs but also the direction of the plastic strain rate vector $\dot{\varepsilon}$ during the flow.

It should be remembered that the J_1/σ_f coordinate is connected with the hydrostatic stress which does not influence the flow of nonporous materials (the Huber-Mises function). The $(J_2')^{1/2}/\sigma_f$ is related to the maximum shear stress at a given plane. Let us identify the direction of the axes J_1/σ_f and $(3J_2')^{1/2}/\sigma_f$ with the direction of $\dot{\varepsilon}_c$ and $\dot{\varepsilon}_s$, the compressive and the shearing strain rates, respectively. By the principle of normality, for any limiting stress conditions determined by the yield surface, the direction of the strain rate $\dot{\varepsilon}$ is normal to the yield locus at the point of tangency. The direction of vector $\dot{\varepsilon}$ is measured by the angle Φ which this vector forms with $\dot{\varepsilon}_s$ (or $(3J_2')^{1/2}/\sigma_f$ axis). For the positive value of Φ the strain rate vector $\dot{\varepsilon}$ has a negative compressive strain rate component $\dot{\varepsilon}_c$. This condition implies the compaction process of a porous body to be characterized by the increase in density (decrease in volume). This behaviour of the porous body is consistent with the actual one during compaction. In contrast the negative value of the angle Φ implies the expansion of the PM material, because the strain rate vector $\dot{\varepsilon}$ has a positive strain rate component $\dot{\varepsilon}_c$ which in this case should be rather named as the tensile strain rate component $\dot{\varepsilon}_t(\dot{\varepsilon}_c = \dot{\varepsilon}_t$ for $\Phi \leq 0)$. Therefore the negative value of Φ results in the decrease of the density of the porous body (increase in volume-dilatancy). From the point of view of an assumed shape of the yield surface for a porous body, two important cases should be discussed:

- for $\Phi = 0$ the strain rate vector $\dot{\varepsilon}$ is parallel to the $(3J_2')^{1/2}/\sigma_f$ axis; it means that no change in volume occurs $(\dot{\varepsilon}_c = 0)$ and the flow is one of pure shear $(\dot{\varepsilon} = \dot{\varepsilon}_s)$.
- for $\Phi = \pi/2$ the strain rate vector $\dot{\varepsilon}$ is perpendicular to the $(3J_2')^{1/2}/\sigma_f$ axis: it means that the shearing component of the strain rate vector is equal to zero $(\dot{\varepsilon}_s = 0)$ and the flow is one of pure hydrostatic $(\dot{\varepsilon} = \dot{\varepsilon}_c)$.

Therefore the shape of the yield surface which describes the deformation of porous material during compaction should also fulfil the following conditions:

$$\begin{aligned} \Phi \to 0 \quad & \dot{\varepsilon}_c \to 0 \\ & \dot{\varepsilon}_s \to \dot{\varepsilon} \\ \Phi \to \pi/2 \quad & \dot{\varepsilon}_s \to 0 \\ & \dot{\varepsilon}_c \to \dot{\varepsilon} \end{aligned} \tag{2}$$

Moreover one also has to recognize that due to further calculations of the incremental strain–stress relations, the mathematical representation of the yield surface should be reasonably simple.

There are three geometrical representations of the yield function for PM materials described in the literature (in σ_1, σ_2, σ_3 coordinates): cap [1], cone [2], and ellipsoid [3–8]. The cap model consists of two parts (Fig. 1): the failure envelope and the cap. The failure surface and the cap are given by Eqs. (3) and (4), respectively.

$$F_1 = (J_2')^{1/2} - [A - C\exp(BJ_1)] \tag{3}$$

$$F_2 = (J_2')^{1/2} - 1/R[(X - L)^2 - (J_1 - L)^2]^{1/2} \tag{4}$$

where:

$$X = L - R[A - C\exp(BL)] \tag{5}$$

The coefficients A, B, C, and R are materials parameters which include a relative density of a porous body. With the function described by Eq. (5) the cap is elliptically shaped and the parameter R is the ratio between the major and minor ellipse axes; X and L define the J_1 range of one semiaxis. One has to recognize that the cap–envelope model admits (depending on where the state of stress is on the yield surface) that the porous body may undergo an increase $(\Phi < 0)$ or decrease in volume $(\Phi > 0)$ during compaction. The increase in the volume of the metal porous body during compaction is inconsistent with the reality and therefore should be excluded from our consideration.

The cone shape of the yield surface is described by the following function:

$$F = (1/A^{1/2})[(3J_2')^{1/2} - BJ_1] \quad (6)$$

The yield function [Eq. (6)] is represented in σ_1, σ_2, σ_3 coordinates by the cone which height increases with increasing ρ. The cone model assumes a constant ratio between the shear $\dot{\varepsilon}_s$ and compressive $\dot{\varepsilon}_c$ component of the plastic strain rate, irrespective of the hydrostatic ($\sigma_m = J_1/3$) and the shear stress (related to J_2').

The inconsistency of the cap and cone model with the real behavior of PM materials during compaction excludes these models from further consideration. The third model discussed in this work is represented in σ_1, σ_2, σ_3 coordinates by an ellipsoid and therefore the yield function is of the following form:

$$F = (1/A^{1/2})(3J_2' + BJ^2)^{1/2} \quad (7)$$

Considering previous requirements, the ellipsoid describes the yield condition for PM materials closest to the actual behavior of the porous body during compaction. First of all, the function [Eq. (7)] fulfils the basic condition of the compaction that any hydrostatic stress is responsible for the volume decrease of the porous material. Moreover, the response of the porous body to the consolidation (compressibility) depends on the ratio between the hydrostatic and shear stresses involved in the process. The coefficients A, B of Eq. (7) are the function of the relative density of PM material. Most of the expressions of A, B variables are based on the experimental results of the simple uniaxial compaction. Only Green[4] applied an analytical approach which considered a uniform cubic array of spherical voids in a solid matrix under states of stress related to pure shear and hydrostatic compaction. The present work also considers the experimental approach to the derivation of A, B variables. This is due to very complicated relationship between the mechanical, rheological and metallurgical factors involved in the forming processes of PM materials. The complexity of compaction, forging, and extrusion of PM materials justifies the experimental approach in order to get the most reliable data for a particular material. I have found such a necessity to derive the new yield function dealing with the optimization of the processing of the 7XXX series PM rapidly solidified aluminum alloys during cold and hot working.

Yield Criterion

The yield criterion for porous materials is proposed of the form:

$$\sigma_p^2 = C\sigma_o^2 = (1/A)(3J_2' + BJ_1^2) \quad (8)$$

σ_p and σ_o are the yield stresses of porous and solid matrix material, respectively. A, B, and C are the functions of the relative density. If σ_p is replaced by $\bar{\sigma}_p$, that is, equivalent stress applied to the porous material, then Eq. (8) may be applicable to the work hardening porous body. Using the concept of plastic potential g, the incremental strain–stress relation is to be derived. The plastic potential g is given with regard to the principal stresses.

$$g = (1/A^{1/2})\{(1/2)[(\sigma_1 - \sigma_2)^2 + (\sigma_2 - \sigma_3)^2 + (\sigma_3 - \sigma_1)^2] + B(\sigma_1 + \sigma_2 + \sigma_3)^2\}^{1/2} - \sigma_p \quad (9)$$

Partially differentiating Eq. (9) with respect to σ_1, σ_2, and σ_3, incremental strain–stress relations can be written as:

$$\begin{aligned} d\varepsilon_1 &= d\lambda'\delta g/\delta\sigma_1 = d\lambda[\sigma_1 - (1 - 2B)\sigma_m] \\ d\varepsilon_2 &= d\lambda'\delta g/\delta\sigma_2 = d\lambda[\sigma_2 - (1 - 2B)\sigma_m] \\ d\varepsilon_3 &= d\lambda'\delta g/\delta\sigma_3 = d\lambda[\sigma_3 - (1 - 2B)\sigma_m] \end{aligned} \quad (10)$$

$d\lambda$ is a proportional factor which is determined after the rearrangement and substitution of Eq. (10) into the expression of plastic work done per unit volume of porous body.

$$dW = \sigma_1 d\varepsilon_1 + \sigma_2 d\varepsilon_2 + \sigma_3 d\varepsilon_3 = \bar{\sigma}_p d\bar{\varepsilon}_p \quad (11)$$

$d\bar{\varepsilon}_p$ is defined as the equivalent strain increment referring to the porous material. Finally the proportional factor $d\lambda$ is described:

$$d\lambda = (3/2A)(d\bar{\varepsilon}_p/\bar{\sigma}_p) \quad (12)$$

Substituting Eq. (12) into Eq. (10), rearranging expression (10) to the form: the principal stress–incremental strain and subsequently substituting into Eq. (11) with the rearrangement:

$$d\bar{\varepsilon}_p = \{A\{(2/9)[(d\varepsilon_1 - d\varepsilon_2)^2 + (d\varepsilon_2 - d\varepsilon_3)^2 + (d\varepsilon_3 - d\varepsilon_1)^2] + (1/9B)(d\varepsilon_v^2)\}\}^{1/2} \quad (13)$$

$d\varepsilon_v$ is volumetric strain increment:

$$d\varepsilon_v = d\varepsilon_1 + d\varepsilon_2 + d\varepsilon_3 = -d\rho/\rho \quad (14)$$

One has to recognize that as in the plasticity theory of solid materials, the concept of equivalent stress and strain is used to correlate the results obtained under different loading conditions by means of a single curve of $\bar{\sigma}-\bar{\varepsilon}$ taken from the simple uniaxial test. In this work $\bar{\sigma}_p$ and $\bar{\varepsilon}_p$ refer to the porous body (suffix p).

This concept introduces the hardening factor of the solid matrix of the porous body and the volumetric hardening due to decrease in the porosity of the PM material during deformation. It is worth mentioning that except for Kuhn's and Downey's theory [3], all the concepts of plasticity theory for porous materials refer to the deformation of the solid matrix material of the porous body, hereby excluding the volumetric work hardening factor. Referring the present theory to the solid matrix material (suffix o) of the porous body one has to introduce:

$$\begin{aligned} \bar{\sigma}_p &= (C)^{1/2}\bar{\sigma}_o \\ d\bar{\varepsilon}_p &= \rho d\bar{\varepsilon}_o \end{aligned} \tag{15}$$

In this case the relationship $\bar{\sigma}_o - \bar{\varepsilon}_o$ is provided by the simple uniaxial test of fully dense materials.

The Upper Bound Theory

The derivation of the upper bound theory for porous metals presented in this paper is based on a general solution for solid materials [9] (Fig. 2). On the body of volume U and total surface area S, let surface stresses or tractions P_i be specified over part of the surface, say SP. Suppose the actual velocity field is denoted V_i^*, any other different or assumed field by V_i, such that $V_i^* = V_i$ on SV, that is, V_i is prescribed over the part of the boundary SV.

A kinematically admissible velocity field may have discontinuities in the tangential component along a certain surface SD. In the upper bound for solid incompressible metals normal components must be the same on the other side of such surfaces in order that there be no plastic volume change.

Denote as $\dot{\varepsilon}_{ij}^*$, the assumed plastic strain rate as derivable from V_i^* and σ_{ij}^*, any stress field which does not violate the yield criterion and is derivable by way of the concept of the plastic potential g.

In Figure 2, V_t^* denotes the tangential component of velocity discontinuity on a surface SD for the kinematically admissible velocity field and q is the shearing stress component of the actual stress field σ_{ij} in the direction of the displacement increment discontinuity.

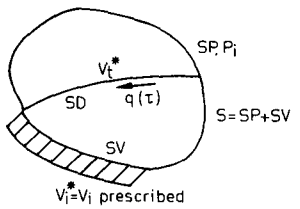

Fig. 2. Terms used in the upper bound theory.

The theory states that among all kinematically admissible velocity fields, the actual one minimize the expression:

$$\dot{W}^* \leq \int_U \sigma_{ij}^* \dot{\varepsilon}_{ij}^* dU + \sum \int_{SD} \tau \mid V_t^* \mid dSD - \int_{SP} P_i V_i^* dSP \tag{16}$$

where τ is the maximum resistance to shear.

The actual externally supplied power $\dot{W}^*$ is never higher than that computed by Eq. (16).

The first term expresses the total power for deforming the body ($\dot{W}_u$).

The second term indicates the internal shear stress along the surface of velocity discontinuity ($\dot{W}_{SD}$), the boundary between the tool and material (friction $\dot{W}_{SF}$ must be specified).

The last term covers power supplied by predetermined body traction SP ($\dot{W}_{SP}$) such as back and front tension in extrusion, drawing, rolling etc. The modification of upper bound for porous materials concerns two first terms [10]. The second term of the right hand side of Eq. (16) must be determined considering the kinematically admissible displacement increment field which has discontinuities not only in the tangential component but also in normal components.

The latter one is responsible for a change in density when the material passes the discontinuity.

In order to simplify the solution, let us assume that the porous body possesses an identical yield surface (between the discontinuity surface) during a deformation process. This identical yield surface implies the constant average relative density of porous material during deformation between two discontinuity surfaces.

It also implies that for the deformation between the discontinuity surfaces $d\varepsilon_u = 0$. Therefore the volume change occurs only as the material passes the discontinuity surface. This assumption is somewhat artificial in character but facilitates simple solutions and reduces the volume of calculations. Otherwise

the exact distribution of density should be known in the body as a continuous function of coordinates, which generally is very difficult or even impossible for working processes such as extrusion, rolling, or forging.

Power for Internal Deformation Over the Volume of the Deforming Body $\dot{W}_u$

Applying Eq. (11) to the first term ($\dot{W}_u$) of the right hand side of Eq. (16), the expression of the power for internal deformation over the volume of the deforming porous body is given:

$$\dot{W}_u = \int_U \bar{\sigma}_p \bar{\dot{\varepsilon}}_p^* dU \tag{17}$$

where $\bar{\dot{\varepsilon}}_p^*$ is equivalent strain rate.

However, following the assumption that for the deformation between the discontinuity surfaces $\dot{\varepsilon}_u^* = 0$ the relative density of the material will be only included into the calculation by coefficient A.

Power Dissipated on the Discontinuity Surfaces $\dot{W}_{SD}$

Geometrical representation of the velocity discontinuity with all the parameters involved is shown in Figure 3.

The surface of velocity discontinuity SD is the central surface of the shaded volume where the velocity changes abruptly. The porous body would undergo discontinuity in velocity in tangential ΔV_t^* and normal ΔV_n^* to the surface of discontinuity. Let x, y, z coordinates be so chosen that the z axis is normal to the surface SD at point 0. According to Figure 3 and the coordinates chosen, velocity components are denoted: $\Delta V_n^* = V_{nz}^*$, ΔV_{tx}^*, ΔV_{ty}^*. Crossing SD the material is distorted owing to the velocity discontinuity and this is subjected to strains $\dot{\varepsilon}_x^*$, $\dot{\varepsilon}_y^*$, $\dot{\varepsilon}_z^*$, $\dot{\gamma}_{xy}^*$, $\dot{\gamma}_{yz}^*$, $\dot{\gamma}_{zx}^*$ per unit time:

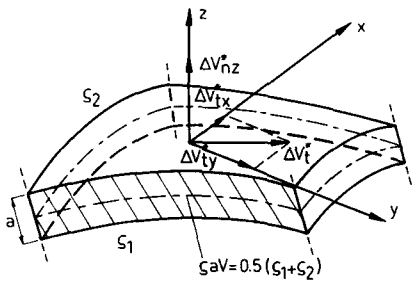

Fig. 3. Surface of velocity discontinuity SD.

$$\begin{aligned}
\dot{\varepsilon}_x^* &= \Delta V_x^*/\Delta x = \dot{\varepsilon}_{tx}^* \\
\dot{\varepsilon}_y^* &= \Delta V_y^*/\Delta y = \dot{\varepsilon}_{ty}^* \\
\dot{\varepsilon}_z^* &= \Delta V_z^*/\Delta z = \dot{\varepsilon}_{nz}^* \\
\dot{\gamma}_{xy}^* &= \Delta V_{tx}^*/\Delta y + \Delta V_{ty}^*/\Delta x \\
\dot{\gamma}_{yz}^* &= \Delta V_{ty}^*/\Delta z + \Delta V_{nz}^*/\Delta y = \Delta V_{ty}^*/a + \Delta V_{nz}^*/\Delta y \\
\dot{\gamma}_{zx}^* &= \Delta V_{nz}^*/\Delta x + \Delta V_{tx}^*/\Delta z = \Delta V_{nz}^*/\Delta x + \Delta V_{tx}^*/a \\
\dot{\varepsilon}_v^* &= \dot{\varepsilon}_x^* + \dot{\varepsilon}_y^* + \dot{\varepsilon}_z^*
\end{aligned} \tag{18}$$

The surface of velocity discontinuity SD may be defined as the narrow shaded volume whose width tends to zero.

The energy dissipated per unit volume time across an area dSD is given by:

$$d\dot{W}_{SD} = \lim_{a \to 0} a\sigma_{ij}\dot{\varepsilon}_{ij}^* dSD \tag{19}$$

However the principle of maximum plastic work imposes:

$$\lim_{a \to 0} a\sigma_{ij}\dot{\varepsilon}_{ij}^* dSD \le \lim_{a \to 0} a\sigma_{ij}^*\dot{\varepsilon}_{ij}^* dSD \tag{20}$$

but following Eq. (11)

$$\sigma_{ij}^*\dot{\varepsilon}_{ij}^* = \bar{\sigma}_p \bar{\dot{\varepsilon}}_p^* \tag{21}$$

Therefore:

$$d\dot{W}_{SD} \le \lim_{a \to 0} a\bar{\sigma}_p \bar{\dot{\varepsilon}}_p^* dSD \tag{22}$$

Employing Eq. (13) for equivalent strain rate of deformation $\bar{\dot{\varepsilon}}_p^*$ in arbitrary Cartesian coordinates

$$\begin{aligned}
\bar{\dot{\varepsilon}}_p^* = (A)^{1/2}\{&(2/9)[(\dot{\varepsilon}_x^* - \dot{\varepsilon}_y^*)^2 + (\dot{\varepsilon}_y^* - \dot{\varepsilon}_z^*)^2 + (\dot{\varepsilon}_z^* \\
&- \dot{\varepsilon}_x^*)^2] + (1/9B)\,\dot{\varepsilon}_v^{*2} + 1/3(\dot{\gamma}_{xy}^{*2} + \dot{\gamma}_{yz}^{*2} + \dot{\gamma}_{zx}^{*2})\}^{1/2}
\end{aligned} \tag{23}$$

with data from Eq. (18), Eq. (22) after rearrangement and integration is given by:

$$\begin{aligned}
\dot{W}_{SD} \le \int_{SD} \bar{\sigma}_p\{&A[(1/9)(4 + 1/B)\Delta V_{nz}^{*2} \\
&+ (1/3)(\Delta V_{tx}^{*2} + \Delta V_{ty}^{*2})]\}^{1/2} dSD
\end{aligned} \tag{24}$$

Power Dissipated on Shear Over Tool–Workpiece Interface W_{SF}

Friction is encountered in forming due to the relative motion between the tool and the material. This friction resistance τ is measured in force units per unit surface area of contact. The surface area of contact is a boundary of the deformed metal. Therefore it is also the shear stress in the material at its boundary. Of the several mathematical descriptions of friction let us employ the description using a constant friction factor m. When a constant friction factor is assumed to exist, the shear stress over a surface is assumed to obey the rule:

$$\tau_o = m\sigma_o/(3)^{1/2} \tag{25}$$

This expression concerns solid material. The resistance to sliding τ_o is proportional to the flow strength of the material σ_o. The shear factor m may have any value between zero and one depending on severity of friction. For frictionless conditions $m = 0$, for sticking friction $m = 1$. For porous materials the expression is modified. Applying the conditions of pure shear ($\sigma_1 = -\sigma_3 = \tau_p$) to Eq. (8) and substituting into Eq. (25)

$$\tau_p = (A/3)^{1/2} m\sigma_p \tag{26}$$

Frictional power losses are computed by integrating the shear stress multiplied by the relative sliding speed. This integration being taken over the area of contact. Therefore for porous material

$$\dot{W}_{SF} = \int_{SF} m\sigma_p (A/3)^{1/2} \Delta V_F^* dSF \tag{27}$$

All calculations of power dissipated over the tool–workpiece interface are derived from the rule that power is force multiplied by velocity. In Eq. (27) ΔV_F^* is a velocity discontinuity tangential to the tool surface.

A Final Upper Bound Solution

Combining all the power during the working, the upper bound solution for porous metals is expressed by:

$$\dot{W} \le \int_u \bar{\sigma}_p \bar{\varepsilon}_p^* dU + \int_{SD} \bar{\sigma}_p \{A[(1/9)(4 + 1/B)\Delta V_{nz}^{*2} + (1/3)(\Delta V_{tx}^{*2} + \Delta V_{ty}^{*2})]\}^{1/2} dSD + \int_{SF} m\sigma_p (A/3)^{1/2} \Delta V_F^* dSF - \int_{SP} P_i V_i^* dSP \tag{28}$$

Determination of B, A, C Variables

The experimental determination of the coefficients A, B, and C concerns the 7XXX series aluminum alloy (Al, Zn 6.0–6.2, Mg 1.9–2.0, Cu 1.7–1.9, Cr 0.2) produced by rapid solidification technology. The extended description of these materials (size distribution, shape, oxidation, microstructures) has been published [11].

The experiment concerns one action compaction of the PM material in a rigid die (Fig. 4). A research set-up equipped with high temperature resistant (up to 873 K) strain gauge transducers provides information about all the stresses involved in the compaction process: compaction pressure σ_1, radial pressure ($\sigma_2 = \sigma_3$), and the pressure transmitted to the lower punch σ_t.

Knowing σ_1 and σ_t, one can estimate the friction between the porous body to be compacted and the surface of the die and punches P_F

$$P_F = (\sigma_1 - \sigma_t)\pi D^2/4 \tag{29}$$

where D is a die diameter.

The experiment was carried out at room and elevated temperatures (473–723 K). The surface of the billet and the tools were extensively lubricated

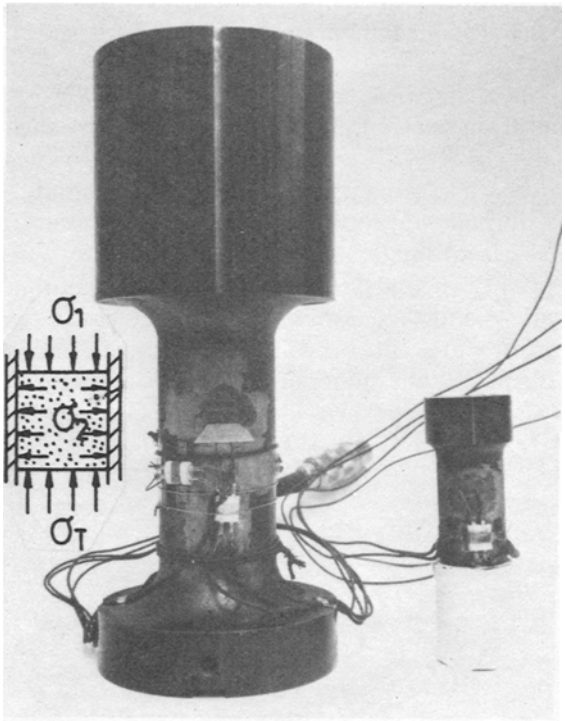

Fig. 4. Die with lower punch.

by graphite in spray in order to reduce the friction during the tests. The billets (dia 30 × 30 mm) were preconsolidated according to the density–pressure relationship (Fig. 5) at room (ρ = 0.70, 0.80, 0.85) and elevated temperatures (ρ = 0.80, 0.85, 0.90, 0.95).

The consolidation of PM materials to higher densities was impossible at room temperature due to a pressure limitation of the press. After preconsolidation the samples were subjected to tests with the research set-up (Fig. 4) at the temperature which assured no change in the sample density.

From the data presented in Figure 5 it is apparent that the density of the porous material depends on the compaction pressure and the temperature within the range up to 473 K. Above this temperature the density depends only on the compaction pressure irrespective of the changes in the temperature of the process.

The microstructures of hot consolidated materials (Fig. 6) reveal the dependence of the porosity level, porosity shape, level of material deformation on the particles morphology, and the compaction pressure. One has to emphasize the importance of the influence of metallurgical properties of PM materials on the flow of porous body during the deformation. Usually this very important factor is not considered by scientists working on the modelling of PM consolidation processes.

Coefficient B

Coefficient B is derived substituting

$$d\varepsilon_2 = d\varepsilon_3 = 0 \qquad \sigma_2 = \sigma_3 \tag{30}$$

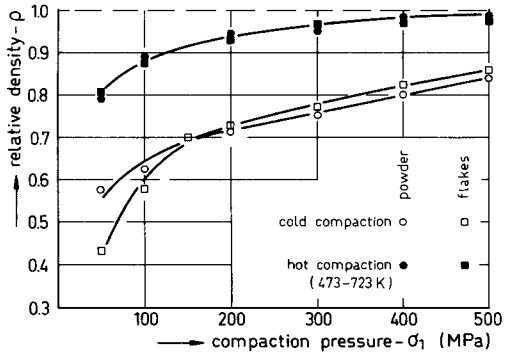

Fig. 5. Relationship: relative density–compaction pressure for cold and hot compaction.

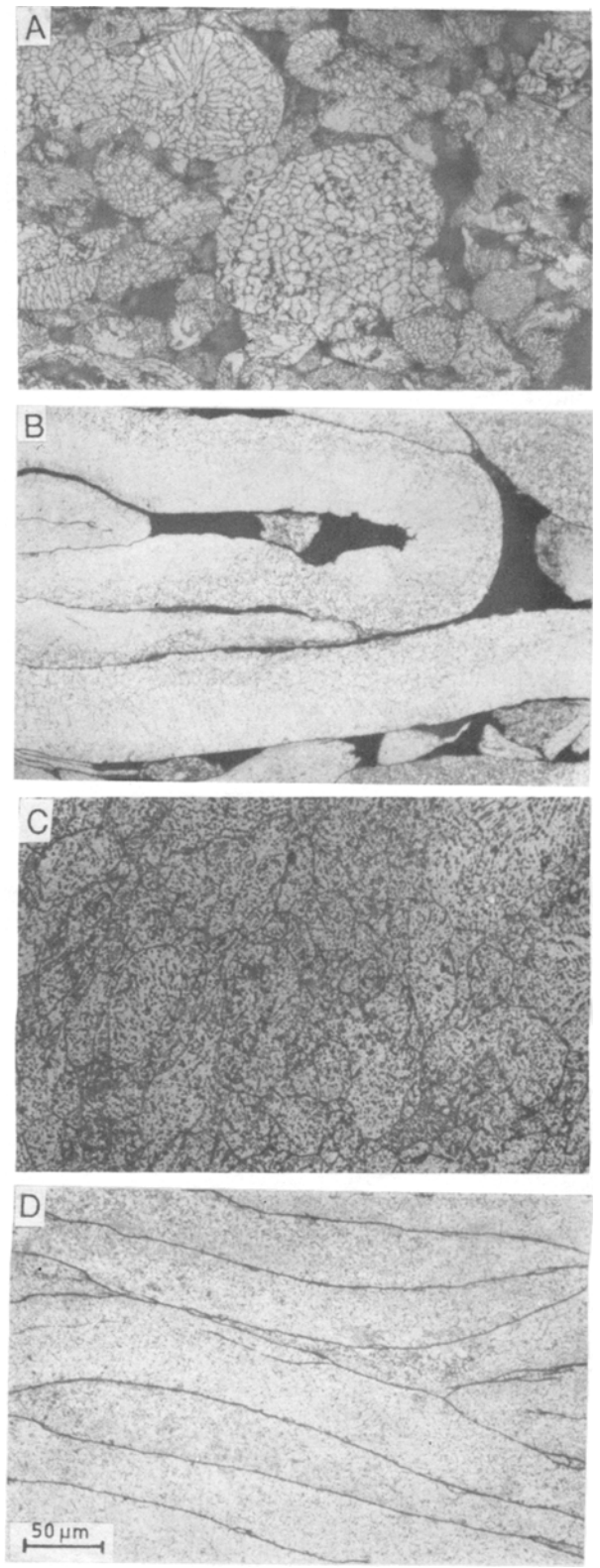

Fig. 6. Microstructures of hot compacted (673 K) billets (powders, flakes) with densities: A, B = 0.9: C, D = 0.99.

into Eq. (10) and rearranging

$$B = [1 - (\sigma_2/\sigma_1)]/2[1 + 2(\sigma_2/\sigma_1)] = f(\rho) \quad (31)$$

σ_2/σ_1 is defined as the coefficient of radial pressure ξ, which is a function of the relative density ρ. From the compaction tests in the rigid die at room and elevated temperatures (Fig. 7) the average relationship between the coefficient of radial pressure and the relative density of the body is found in the form:

- for cold compaction (CC) within the range of relative density $0.7 \leq \rho \leq 0.85$

$$\xi = 0.2\,\rho + 0.4 \quad (32)$$

- for hot compaction (HT, temperatures 473–723 K) within the range of relative density $0.8 \leq \rho \leq 1$

$$\xi = 2.5\,\rho - 1.5 \quad (33)$$

Separately substituting Eqs. (32) and (33) into Eq. (31):

$$B = (0.3 - 0.1\rho)/(1.8 + 0.4\rho) \quad (34)$$

$$B = 1.25(1 - \rho)/(-2 + 5\rho) \quad (35)$$

for cold compaction within the density range $0.7 \leq \rho \leq 0.85$ [Eq. (34)] and for hot compaction with density $0.80 \leq \rho \leq 1.0$ [Eq. (35)].

It is apparent that Eq. (32) for cold compaction when substituted into Eq. (31) with $\rho = 1$ does not fulfil the preliminary condition $B = 0$ (the Huber-Mises form of the yield function). For the compaction of the green body it is consistent with reality because this process involves not only the effect of plastic deformation of particles but also the interparticle sliding. Therefore in this particular case the yield stress σ_p defined by Eq. (8) appears to be a material constant Y which refers to the resistance of powder to compaction, including both plastic deformation and interparticle sliding. Applying this approach, the $\sigma_p = Y$ value for cold compaction of green compacts is to be determined from the rigid die compaction tests substituting the relations [Eq. (34)] $\sigma_2 = \sigma_3 = \xi\sigma_1$ and $A = 1 + B$ (from the simple uniaxial compaction) into Eq. (8). This procedure should give Y data with regard to the density including the work hardening due to decrease in the porosity during compaction. For the 7XXX series PM rapidly solidified aluminum alloy considered in this work, the value of the Y variable estimated with the data from the rigid die compaction is listed in Table 1.

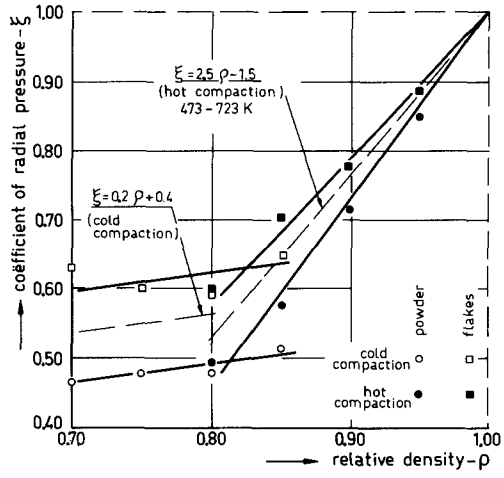

Fig. 7. Relationship coefficient of radial pressure–relative density for cold and hot compaction.

Tackling the experimental data presented in Figure 7 , one has to recognize the different behavior of flakes and powders during cold and hot compaction. In general, the flake material due to lower oxidation, finer microstructure, and better flow properties [11], more homogeneously distributes applied stresses during the consolidation giving a much higher value of the coefficient of radial pressure than the powder particles. Moreover, it is also apparent that hot compaction improves the homogenity of stress distribution compared to that of cold compaction. However, one has to emphasize that the value for the given density is not dependent on the temperature within the range 473–723 K.

Coefficient A

The coefficient A is derived by the adjustment of Eq. (8) to the conditoin of simple uniaxial compaction ($\sigma_p = \sigma_1$; $\sigma_2 = \sigma_3 = 0$). Therefore:

$$A = 1 + B \quad (36)$$

Substituting Eq. (34) or (35) into Eq. (36) one obtains the A value for cold and hot forming processes respectively, with regard to the prescribed density range.

Table 1. Parameter Y Characterized Resistance of Powders to Cold Compaction

σ, MPa	150	250	400	500
density, ρ	0.70	0.75	0.80	0.85
Y, MPa	119	195	309	383

Coefficient C

The coefficient C relates the yield stress of the porous body with the yield stress of the nonporous fully dense matrix material. Tackling the problem of the yield stress of the porous body it is apparent that total strain of deformation, strain rate, temperature, relative density and microstructure of the material should be considered. Due to the very complex relationship among the above-mentioned factors, the present study considers only some of them throughout the experimental tests with simple uniaxial compaction conducted on a standard tensile machine and hydraulic press according to the standard procedure. The tests have been carried out with different temperatures, strain rates, and relative densities of the billets. Prior to the simple uniaxial compaction the billets have been consolidated in the rigid die at the temperature of the uniaxial test. A hot working temperature of 673 K has been selected for subsequent verification tests (Fig. 8). The experiment (Fig. 8) provides for this particular temperature the following relations between coefficient C and the density for the prescribed strain rates $\dot{\varepsilon}$ of hot forming:

$$\begin{aligned} &(\dot{\varepsilon} = 1\ \text{sec}^{-1}) && C = 2.78\,(\rho - 0.4)^2 \\ &(\dot{\varepsilon} = 0.1\ \text{sec}^{-1}) && C = 4\,(\rho - 0.5)^2 \\ &(\dot{\varepsilon} = 0.01\ \text{sec}^{-1}) && C = 6.25\,(\rho - 0.6)^2 \end{aligned} \tag{37}$$

Therefore the relationship between the yield stress of porous body σ_p and fully dense material σ_o is of the form:

$$\begin{aligned} \sigma_p &= 1.67\,(\rho - 0.4)\sigma_o \\ \sigma_p &= 2.0\,(\rho - 0.5)\sigma_o \\ \sigma_p &= 2.5\,(\rho - 0.6)\sigma_o \end{aligned} \tag{38}$$

for $\dot{\varepsilon} = 1\ \text{sec}^{-1}$, $0.1\ \text{sec}^{-1}$, $0.01\ \text{sec}^{-1}$, respectively.

The relations (38) should be applied with regard to the value of strain rate of the deformation, typical for the particular kind of forming process. Hence a strain rate of $\dot{\varepsilon} = 1\ \text{sec}^{-1}$, $0.1\ \text{sec}^{-1}$, $0.01\ \text{sec}^{-1}$ should be considered for the extrusion, compaction with hydraulic press, and isostatic pressing, respectively.

In Figure 9 the yield function is represented at various density levels in $(3J_2')^{1/2}/\sigma_f$ versus J_1/σ_f spaces with regard to yield stress of a porous body ($\sigma_f = \sigma_p$) or solid matrix of a porous material ($\sigma_f = \sigma_o$) at a strain rate of deformation $\dot{\varepsilon} = 1\ \text{sec}^{-1}$ and temperature 673 K. The yield criterion both for σ_p and σ_o follows the pattern described in the literature [6] approaching the Huber-Mises criterion when $\rho = 1$.

However, Figure 9 reveals one interesting feature of the criterion dealing with the porous body (σ_p). At low values of the first invariant of stress tensor J_1, the yielding ellipsoid provides $(3J_2')^{1/2}/\sigma_p$ higher than 1 for $\rho < 1$. The lower the density, the higher the discrepancy between the von Mises cylinder and the ellipsoid at $J_1/\sigma_p = 0$. This behavior of the yield surface for a porous body at the low values of J_1 may result from the discrepancy between the idealized theoretical model which concerns conditions of pure plastic deformation and the actual experiment which provided the coefficient B. The actual experiment also includes a certain level of interparticle sliding. The lower the density, the more likely is interparticle sliding to occur as a predeformation step. One should also be aware that below a threshold stress level it

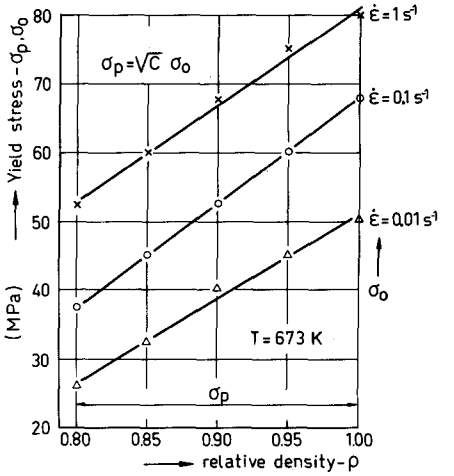

Fig. 8. Relationship: yield stress (porous body σ_p, solid matrix σ_o)–density ρ at different strain rate $\dot{\varepsilon}$ of hot forming ($T = 673$ K).

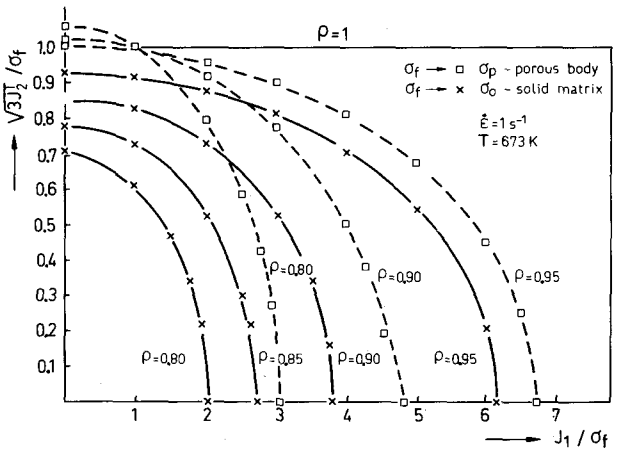

Fig. 9. Yield surface for the yield criterion related to the deformation of porous body σ_p or to the deformation of solid matrix of porous body σ_o.

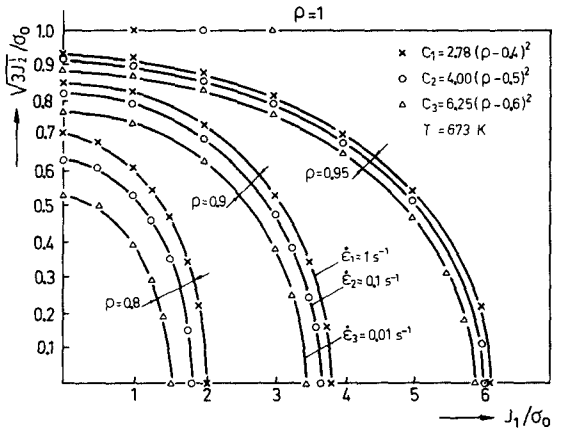

Fig. 10. Yield surface for the yield criterion related to the deformation of solid matrix of porous body σ_o at different strain rate $\dot{\varepsilon}$.

is difficult to proceed with the deformation of a porous body at all. This behavior of the yield surface, although only reported in the literature for Kuhn's theory [12] is common for all the yield criteria after their arrangement with regard to the deformation of the whole porous body [6]. When the yield criterion is presented with regard to a deformation of a solid matrix of a porous body, the $(3J_2')^{1/2}/\sigma_o$ is always lower than 1 for the $\rho < 1$. This behavior is also presented in Figure 10 for a different strain rate of deformation $\dot{\varepsilon}$ at 673 K.

Experimental Verification

Cold Isostatic Compaction

If the pressure during cold isostatic compaction of the 7XXX PM rapidly solidified aluminum powder is denoted by p, that is

$$\sigma_1 = \sigma_2 = \sigma_3 = p \tag{39}$$

then Eq. (8) is of the following form:

$$\sigma_p = Y = 3\,(B/A)^{1/2}p \tag{40}$$

Substituting Y (Table 1), B [Eq. (34)] and $A = 1 + B$, the relationship between the density ($0.70 \leq \rho \leq 0.85$) and the pressure can be estimated. Figure 7 shows the experimental and the estimated relationship: relative density–pressure in cold isostatic compaction of the 7XXX series PM rapidly solidified aluminum alloy material. The points indicate the estimated data using the functions which have been determined by means of rigid die compaction tests. The experimental results agree well with the theoretical ones confirming validity of the presented approach provided the density range $0.70 \leq \rho \leq 0.85$.

This comparison proves that the functions derived using rigid die compaction tests can be applicable to other cold consolidation processes of the 7XXX series PM aluminum alloys within the density range $0.70 \leq \rho \leq 0.85$.

Tackling the density–pressure relationship in the cold rigid die compaction (Fig. 5) and cold isostatic pressing (Fig. 11) it is apparent that the pressure required for full densification of the porous body increases beyond that obtainable by commercial presses. Moreover, for the high compacting pressure (σ_1, $p \geq 300$ MPa) both cold rigid die and cold isostatic compaction produce similar green densities. It is due to the increase of the coefficient of radial pressure with the increase of the relative density during cold compaction in the rigid die. Merely the pressure distribution becomes more homogeneous and therefore closer to that observed during cold isostatic pressing. Moreover, a certain amount of shearing stresses consistent with the rigid die compaction helps to densify powders [13].

Hot Uniaxial Compaction (Simple Uniaxial Compression)

The verification of the presented theory has also been carried out for hot deformation processes. In this work the comparison between estimated and experimental values of Poisson's ratio ν from standard simple hot uniaxial frictionless compaction (T = 673 K, $\dot{\varepsilon} = 0.01\ \text{sec}^{-1}$) is presented. Poisson's ratio is determined experimentally from the relationship

$$\nu = -d\varepsilon_2/d\varepsilon_1 \tag{41}$$

The value of σ_1, applied during hot uniaxial com-

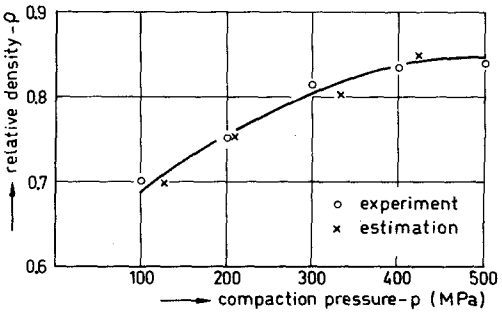

Fig. 11. Experimental and estimated relationship: relative density–compaction pressure during cold isostatic pressing.

paction, coincides with σ_1 used during hot preconsolidation of the test samples in the rigid die. The estimation of Poisson's ratio has been carried out applying the functions from the rigid die tests with conditons $d\varepsilon_2 = d\varepsilon_3$ and $\sigma_2 = \sigma_3 = 0$ substituted into Eq. (10).

After the rearrangement:

$$\nu = (1 - 2B)/2(1 + B) \tag{42}$$

where B is the function of initial density of a porous body described by Eq. (35).

It is apparent from Figure 12 that calculated data fit very well to the experimental ones.

The relationship between Poisson's ratio and the density can be described by:

$$\nu = 0.5\ \rho^a \tag{43}$$

where $a = 1.6$ and 1.7 for the estimated and experimental results, respectively. A similar relationship ($\nu = 0.5\ \rho^2$) has been found by Kuhn [12] for hot deformation (644 K) of the 601 AB (Al, 0.25 Cu, 0.6 Si, 1.0 Mg) PM aluminum porus body.

Extrusion

Application of the proposed upper bound theory for an extended calculation of extrusion pressures is presented elsewhere [14]; however, in this work the basic assumption concerning the relationship between velocity discontinuities and densification will be discussed for the extrusion of PM rapidly solidified 7XXX series aluminum flakes.

The flakes were first compacted to 0.80 theoretical density. The billets were subsequently extruded till the beginning of the steady state extrusion when material just starts to exit from the die. The extrusion was performed at 673 K through a flat die with a reduction ratio $R = 20$. The microstructures, hardness, and density were investigated providing data which are presented in Figures 13 and 14.

Considering these properties throughout the longitudinal plane of the discard one can distinguish five regions:

1. The compaction zone of a spherical shape with the very low intensity of shearing stresses resulting in the lowest microhardness and low density.
2. The intermediate zone where one can observe a rearrangement of flakes due to an increase of the intensity of shearing stresses which, however, results only in insignificant increase in density.
3. The hardening zone where the intensity of shearing stresses is high and this results in the highest value of microhardness and significant increase in density.
4. The tensile zone with the low intensity of shearing stresses and a very high intensity of tensile stresses. The influence of tensile stresses is observed through an occurrence of large cracks propagated from a corner between the liner and the die. This zone is related with the dead metal zone. The density is the lowest due to macrodefects.
5. The softening zone created close to the exit and to the wall of the due. This zone is consistent with an elevated temperature of the process and a sig-

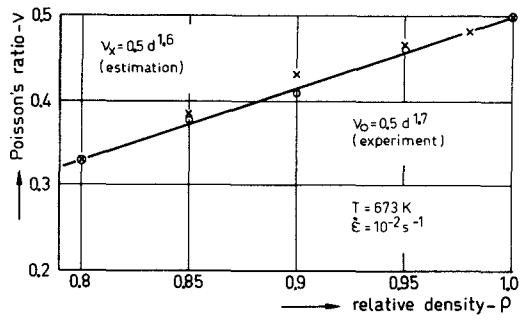

Fig. 12. Experimental and estimated relationship: Poisson's ratio–relative density during simple uniaxial compaction.

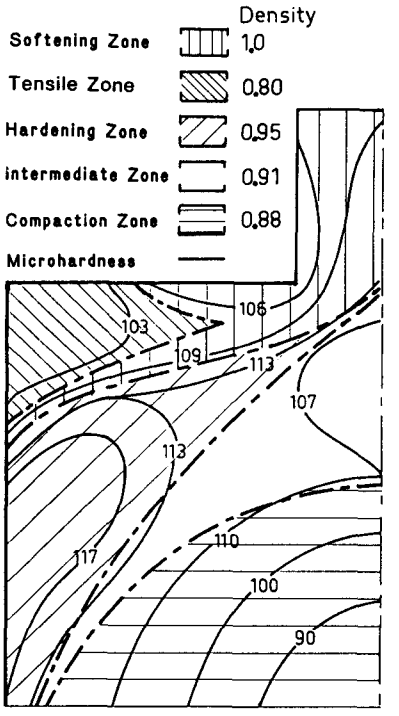

Fig. 13. Microhardness distribution in the discard.

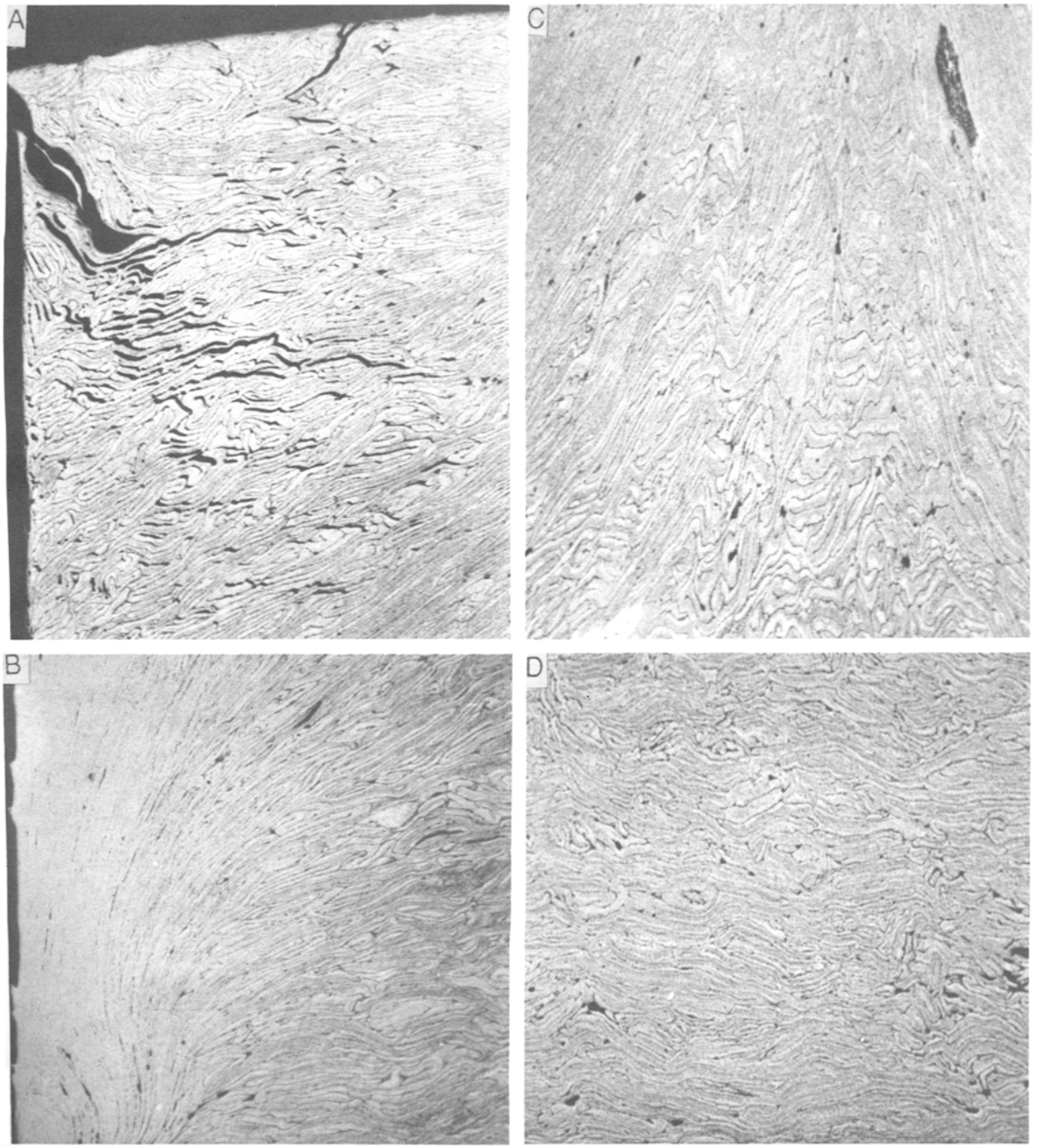

Fig. 14. Microstructure of the billet to be extruded (20X): (A) tensile zone–dead metal zone, (B) vicinity of the liner and ram, (C) end of intermediate zone, (D) compaction zone.

nificant rise in temperature due to the high intensity of shearing stresses. The density of this zone approaches the theoretical one.

The microstructures reveal the effect of shear forces arising from the friction at the tool–billet interface and its significant influence on the displacement of flakes and the densification of the billet. One can recognize that there is relationship between the level of shearing and the level of densification. The higher the shearing stresses the higher the local density of the billet. Moreover the shape of the zones with sig-

nificant differences in density could be approximated to simple geometrical ones (i.e., spherical). It indicates that the assumption that the porous body may be characterized by the existence of displacement rate discontinuities can be acceptable.

Conclusions

The satisfactory level of correlation between the experimental and calculated data indicates that the yield criterion with the material constants determined from the rigid die compaction tests at room and elevated temperatures can be used to analyze various compaction processes of porous materials.

The application of the yield criterion to the upper bound solution seems to be also satisfactory.

The microstructures, density, and hardness data throughout the deformation zone during the hot extrusion indicate that the porous body may be characterized by the existence of displacement discontinuities. The experiment shows different behavior of PM material during hot and cold compaction. The main difference concerns the fact that during cold pressing of the green billet, except in the plastic deformation of powders, interparticle sliding is additionally involved in the process.

The experimental approach to the derivation of the yield function for PM materials and the upper bound solution is justified due to complex mechanical, rheological, and metallurgical characteristics of PM materials involved in the different forming processes.

Acknowledgments. The author is indebted to Mr. T.L.J. de Haan for his skillful assistance with optical microscopy. Thanks are also due to Professors P. Jongenburger and B.M. Korevaar for stimulating discussion.

Financial support of the Programme for Innovative Research Metals in the Netherlands is gratefully acknowledged.

References

1. M. Heheberger and P. Lindskog: Proc. of Powder and Pressing Technology Seminar, Sandviken, 1985, pp. 1–16.
2. F. Tabata and S. Masaki: *Int. J. Mech. Sci.*, 1977, vol. 20, pp. 505–512.
3. H.A. Kuhn and C.L. Downey: *Int. J. Powder Metallurgy*, 1971, vol. 7, pp. 15–25.
4. R.J. Green: *Int. J. Mech. Sci.*, 1972, vol. 14, pp. 215–224.
5. S. Shima and M. Oyane: "Plasticity Theory for Porous Materials," *Int. J. Mech. Sci.*, 1976, vol. 18, pp. 285–291.
6. S.M. Doraivelu, H.L. Gegel, J.S. Gunasekera, J.C. Malas, and J.T. Morgan: A New Yield Function for Compressible PM Materials, *Int. J. Mech. Sci.*, 1984, vol. 26, pp. 527–535.
7. I.F. Martynova and M.B. Shtern: *Poroshkovaya Metallurgiya*, 1978, No. 1 (181), pp. 23–29.
8. M.B. Shtern: *Poroshkovaya Metallurgiya*, 1981, No. 4 (220), pp. 17–23.
9. W. Johnson and B.P. Mellor: *Plasticity for Mechanical Engineers*, London, P. van Nostrad Comp. Ltd., 1970, pp. 289–291.
10. S. Shima, T. Tabata, M. Oyane, and T. Kawakami: *Memoirs of the Faculty of Engineering*, Kyoto University, 1976, vol. 38, pp. 117–137.
11. J. Duszczyk and P. Jongenburger: *Powder Metallurgy*, 1986, vol. 29, pp. 20–26.
12. H. Kuhn: *Power Metallurgy Processing*, Academic Press, New York, 1978, pp. 99–138.
13. J. Duszczyk: *Int. J. Powder Metallurgy and Powder Technology*, 1984, vol. 20, pp. 103–114.
14. J. Duszczyk and L. Kowalski: *J. Mater. Shaping Technology*, 1990, vol. 8, pp. 225–237.